Seatific Journal
https://seatific.yildiz.edu.tr
DOI: https://doi.org/10.14744/seatific.2024.0001

Research Article

A numerical study about the influence of bathymetry on the generation and propagation of realistic irregular waves and representative regular waves occurred in Tramandaí, Brazil

Ana Paula Giussani MOCELLIN[1], Maycon da Silveira PAIVA[1], Elizaldo Domingues DOS SANTOS[1], Luiz Alberto Oliveira ROCHA[1], Liércio André ISOLDI[1], Juliana Sartori ZIEBELL[2], Bianca Neves MACHADO*[3]

[1]*School of Engineering, Federal University of Rio Grande, Rio Grande do Sul, Brazil*
[2]*Department of Pure and Applied Mathematics, Federal University of Rio Grande do Sul, Rio Grande do Sul, Brazil*
[3]*Interdisciplinary Department, Federal University of Rio Grande do Sul, Rio Grande do Sul, Brazil*

ARTICLE INFO

Article history
Received: March 22, 2024
Revised: April 10, 2024
Accepted: April 17, 2024

Key words:
Realistic irregular waves; representative regular waves; WaveMIMO methodology; bathymetry; wave energy

ABSTRACT

Due to the increase in global energy consumption and the search to diversify the energy matrix, an increase has occurred in research related to renewable energy sources. In this regard, the energy contained in sea waves stands out. Therefore, this study aims to analyze the influence of wave channel bathymetry on the generation and propagation of realistic irregular waves and representative regular waves in the sea conditions occurring in Tramandaí in the state of Rio Grande do Sul, Brazil. Toward this aim, the study considers two geometries for the wave channel: one with a flat bottom and one with an inclined bottom (representing local bathymetry). In order to numerically simulate the wave channels, the study employs the computational fluid dynamics software Ansys Fluent, which is based on the finite volume method. The volume of fluid (VOF) model was used for the treatment between the phases, which are water and air. The WaveMIMO methodology has been used to generate realistic irregular waves while Stokes second-order wave theory was taken into considered for generating the representative regular waves. In this way, the study has been able to determine the use of a channel with an inclined bottom to lead to more accurate results, as the evaluated metrics show improvements of around 0.3% regarding realistic irregular waves and up to 2.0% regarding representative regular waves.

Cite this article as: Mocellin APG, Paiva MDS, Dos Santos ED, Rocha LAO, Isoldi LA, Ziebell JS, Machado BN. A numerical study about the influence of bathymetry on the generation and propagation of realistic irregular waves and representative regular waves occurred in Tramandaí, Brazil. Seatific 2024;4:1:1–11.

1. INTRODUCTION

Renewable energy sources are of extreme importance, whether in the environmental, social, economic, or political environment of a country, especially when geopolitical conflicts continue to affect the energy sector worldwide (Santana, 2023). According to Santana (2023), the commitment to this kind of energy is furthermore evident when observing the debate surrounding it today, which prioritizes sustainability through projects that aim to reduce and replace fossil fuels with clean energy that does not harm the environment.

In fact, the interest in renewable energy has been growing annually, as shown in the Renewables 2023 report (International Energy Agency, 2024), which points to a

***Corresponding author.**
*E-mail address: bianca.machado@ufrgs.br

growth of around 50% in the annual global capacity for renewable electrical energy production when compared to 2022. Even so, continuing to search for how to diversify energy matrices is important. For instance, 47.4% of the energy made available in 2022 in Brazil came from renewable sources. When considering electrical energy, however, 61.9% of the energy produced is concentrated in the hydroelectric sector (Energy Research Office, 2023).

One alternative that has yet to be fully explored worldwide is marine renewable energy, which is present in the oceans in different forms and among which wave energy stands out (Cisco et al., 2020). This kind of energy can be extracted through the use of wave energy converter devices such as an oscillating water column (OWC), overtopping, oscillating bodies (Pecher & Kofoed, 2017), or a submerged horizontal plate (Seibt et al., 2023).

Studies on technologies for converting sea wave energy into electric energy have been advancing in recent years. Inside the numerical field, simulations for generating and propagating waves in channels have been carried out by considering the incidence of such waves over the converter devices. This enables evaluating device performance without the costs associated with laboratory experiments and real prototypes. However, the literature shows no consensus regarding how to configure the bottom of the numerical wave channels considered in these simulations, namely whether these should be considered with a flat or with an inclined bottom to reproduce local coastal bathymetry.

For instance, several studies can be found to have considered both approaches for wave channel bottoms. For example, Palma et al. (2019) studied the hydraulic performance of the Overtopping BReakwater for wave Energy Conversion (OBREC) device, which consists of breakwater with an integrated overtopping converter while considering a wave channel with a flat bottom. Hübner et al. (2022) also evaluated the performance of an overtopping device being subjected to different wave climates based on realistic sea state data referring to three coastal municipalities; they considered the bathymetry of each location when employing numerical channels with inclined bottom. Koch et al. (2021) analyzed the performance of an OWC device under the incidence of representative regular and realistic irregular waves by also considering a channel with an inclined bottom. Meanwhile, Cannata et al. (2023) carried out a numerical investigation on the efficiency of a OWC device subjected to regular and irregular waves whose wave channel had a flat bottom. Maciel et al. (2023) carried out the geometric optimization of an OWC device in order to maximize the hydro-pneumatic power obtained by a converter subject to realistic irregular waves by considering a channel with a flat bottom.

By aiming to contribute to the research of sea wave energy conversion devices, the present study is dedicated to improving the generation and propagation of numerical waves, which is a fundamental aspect for studies carried out in this field. The following are examples of studies dedicated to the generation and propagation of waves. Machado et al. (2021) presented and verified the WaveMIMO methodology for wave generation using discrete transient data as the prescribed velocity boundary condition (BC). Maciel et al. (2021) verified and validated the WaveMIMO methodology by comparing numerically obtained results with those from experimental studies. Paiva et al. (2023) evaluated the discretization of the region of imposition for the prescribed velocity BC, which is a necessary step for using the WaveMIMO methodology.

In this context, the present study aims to provide a recommendation regarding whether or not to use the local bathymetry at the bottom of wave channels considered in numerical simulations that are performed for investigating wave energy conversion devices. Thereby, this study carries out simulations on generating and propagating realistic irregular waves and representative regular waves by considering channels with flat bottoms and channels with inclined bottoms. Finally, the waves generated in the present paper should be highlighted as having been based on the sea conditions occurring in 2018 in the municipality of Tramandaí, located in the state of Rio Grande do Sul (RS), Brazil.

2. MATHEMATICAL AND COMPUTATIONAL MODELING

The study performs numerical simulations of wave generation in channels by means of the fluid dynamics software Ansys Fluent based on the finite volume method (Maliska, 2004). The volume of fluid (VOF) model as proposed by Hirt & Nichols (1981) is taken into consideration for handling the air and water phases. The model represents the water and air phases through the concept of the volumetric fraction (α), where the sum of the phases in each volume must always be unitary. As such, each computational cell might be in one of three different states. The first contains both phases and is expressed as:

$$\alpha_{water}+\alpha_{air}=1 \quad (1)$$

The second contains just water and is expressed as:

$$\alpha_{water}=1 \quad (2)$$

The third contains just air and is expressed as:

$$\alpha_{\text{air}}=1 \quad (3)$$

Moreover, because the VOF model is used for immiscible fluids (i.e., fluids that do not mix), from Eq. 1 it is possible to define that:

$$\alpha_{water}=1-\alpha_{air} \quad (4)$$

When employing the VOF model, a single set of equations is used that are composed of the conservation of mass, volume fraction, and momentum equations. This set of equations is thus represented in order as (Versteeg & Malalasekera, 2007):

$$\frac{\partial(\rho)}{\partial t}+\nabla.(\rho\vec{v})=0 \quad (5)$$

$$\frac{\partial(\alpha)}{\partial t}+\nabla.(\alpha\vec{v})=0 \quad (6)$$

$$\rho\frac{\partial}{\partial t}(\vec{v})+\rho(\nabla.\vec{v})\vec{v}=-\nabla.p+\nabla.(\bar{\bar{\tau}})-\rho\vec{g}+S \quad (7)$$

where, ρ is the fluid density (kg/m³); t is the time (s); $\vec{v}$ is the velocity vector (m/s), p is the static pressure (N/m²), $\bar{\bar{\tau}}$ is the stress deformation tensor (N/m²), and $\vec{g}$ is the gravity acceleration vector (m/s²). Furthermore, S is the term sink, which refers to the numerical beach tool and is used to avoid the reflection of waves when hitting the end of the channel. It is calculated as follows (Lisboa et al., 2017):

$$S = -\left[C_1\rho V + \frac{1}{2}C_2\rho|V|V\right]\left(1-\frac{z-z_{fs}}{z_b-z_{fs}}\right)\left(\frac{x-x_s}{x_e-x_s}\right)^2 \quad (8)$$

where C_1 and C_2 are the linear (s⁻¹) and quadratic (m⁻¹) damping coefficients, respectively; x is the horizontal position, z is the vertical position, V is the velocity along the z direction (m/s), z_{fs} and z_b are the respective vertical positions of the free surface and bottom (m), and x_s and x_e are the respective horizontal positions of the beginning and end of the numerical beach (m). Finally, the damping coefficients C_1 and C_2 are worth mentioning to have been defined in accordance with Lisboa et al. (2017) as 20 s⁻¹ and 0 m⁻¹, respectively.

2.1. Generation of the realistic irregular waves

In order to enable the numerical generation of realistic irregular waves, the study uses the WaveMIMO methodology (Machado et al., 2021), which consists of how the spectral data are handled. In the present study, these data come from the TELEMAC-based operational model addressing wave action computation (TOMAWAC) spectral model. TOMAWAC is used in order to transform this spectrum into a time series of free surface elevations that are approximated through a finite sum of monochromatic waves using the Spec2Wave software (Oleinik, 2022).

This time series is handled appropriately so as to obtain the horizontal (u) and vertical (w) components of the orbital velocity of the water particle propagation (Oleinik et al., 2021), which are then imposed as prescribed velocity BC in Ansys Fluent. The velocity profiles associated with each of the monochromatic waves are given as follows (Dean & Dalrymple, 1991):

$$u = \frac{H}{2}\frac{gk}{\sigma}\frac{\cosh(kz+kh)}{\cosh(kh)}\cos(kx-\sigma t) \quad (9)$$

$$w = \frac{H}{2}\frac{gk}{\sigma}\frac{\sinh(kz+kh)}{\cosh(kh)}\sin(kx-\sigma t) \quad (10)$$

where, H is the wave height (m), h is the depth (m), and k is the wavenumber (m⁻¹), given by:

$$k = \frac{2\pi}{\lambda} \quad (11)$$

with λ being the wavelength (m) and σ the angular frequency (Hz), as given by:

$$\sigma = \frac{2\pi}{T} \quad (12)$$

where T is the wave period (s).

Both examinations considered the sea state data that occurred in Tramandaí on May 28, 2018 at 10:14 AM, at a point located 2,094.33 m off the coast at the geographic coordinates of -50°06'18"W -29°59'52"S. Thus, the aim of selecting the wave spectrum that best represents the wave climate, realistic data of significant height (H_s), and mean period (T_m) that occurred at the noted location is to analyze both cases comparatively. Thus, Figure 1 presents a bivariate histogram relating to the occurrences of H_s and T_m and indicates the most frequent combination.

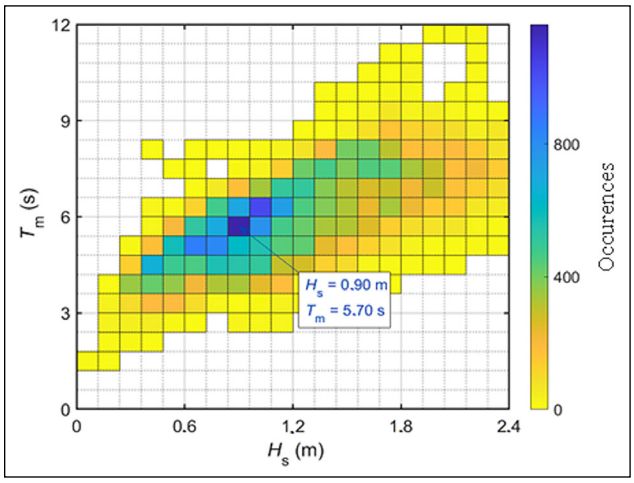

Figure 1. Bivariate histogram of H_s and T_m.

2.2. Generation of the representative regular waves

Knowing the most frequent H_s and T_m characteristics of the analyzed sea state, as well as the depth of the region chosen for the study enables the wavelength of the representative regular waves of this sea state to be determined. Therefore, the study employs the dispersion relationship, which is expressed as (Dean & Dalrymple, 1991):

$$\sigma^2 = gk\tanh(kh) \quad (13)$$

Finally, Table 1 shows the characteristics of the representative regular waves being considered in the present study. These characteristics should also be noted as being considered for both the spatial and temporal discretization of the computational domains that are used, as will be addressed later.

According to Chakrabarti (2005), such waves are classified as second-order Stokes waves. Therefore, the free surface elevation is analytically described as follows (Dean & Dalrymple, 1991):

$$\eta = \frac{H}{2}\cos(kx-\sigma t) + \frac{H^2k}{16}\frac{\cosh(kh)}{\sinh^3(kh)}[2+\cosh(2kh)]\cos[2(kx-\sigma t)] \quad (14)$$

while, the horizontal and vertical propagation velocities are described, respectively, by Dean & Dalrymple:

$$u = \frac{H}{2}\frac{gk}{\sigma}\frac{\cosh(kz+kh)}{\cosh(kh)}\cos(kx-\sigma t) + \frac{3}{16}H^2\sigma k\frac{\cosh[2k(h+z)]}{\sinh^4(kh)}\cos 2(kx-\sigma t) \quad (15)$$

$$w = \frac{H}{2}\frac{gk}{\sigma}\frac{\sinh(kz+kh)}{\cosh(kh)}\sin(kx-\sigma t) + \frac{3}{16}H^2\sigma k\frac{\sinh[2k(h+z)]}{\sinh^4(kh)}\sin 2(kx-\sigma t) \quad (16)$$

Table 1. Characteristics of the representative regular waves

Characteristic	Nomenclature	Magnitude
Significant height	H_s (m)	0.90
Wavelength	λ (m)	45.91
Mean period	T_m (s)	5.70
Depth	h (m)	10.98

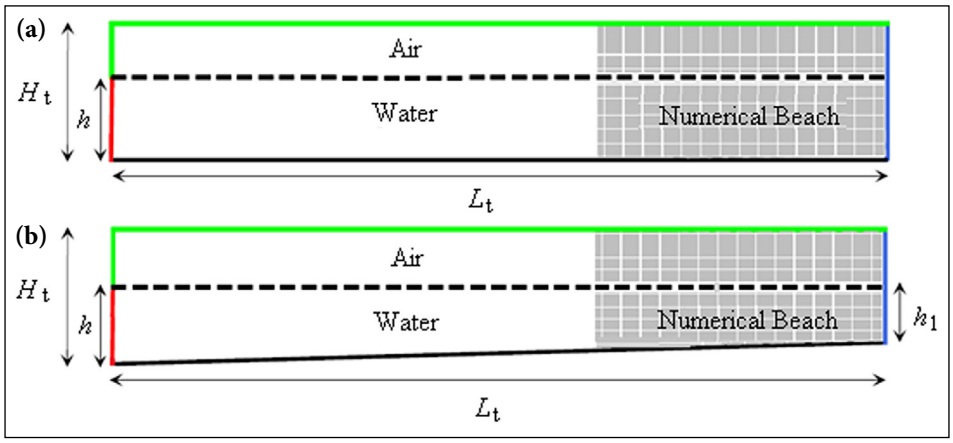

Figure 2. Computational Domain used in the study: (a) flat bottom; (b) inclined bottom.

3. PROBLEM DESCRIPTION

As mentioned previously, the objective of the present study is to analyze whether the use of bathymetry affects the generation and propagation of realistic irregular waves and representative regular waves. Toward this aim, the study takes two computational domains into consideration: 1) domains with a flat bottom (Fig. 2a), where bathymetry data is not considered, and 2) domains with an inclined bottom (Fig. 2b) that reproduces the local bathymetry found off the coast of Tramandaí.

Consequently, both wave channels have basically the same dimensions: length, L_t= 229.56 m, which corresponds to 5λ and is in accordance with the recommendation of Gomes et al. (2012); height, H_t=15.00 m; and depth h=10.98 m. Depth h is constant for cases with a flat bottom, and variable for cases with an inclined bottom, with h=10.98 m at the left side of the wave channel and h_1=10.52 m at the right side. Finally, the bathymetric data should be noted as having been obtained from the Hydrography and Navigation Directorate of the Brazilian Navy's nautical charts, as cataloged by Cardoso et al. (2014).

In regards to the BC, both cases considered the following (Fig. 2): atmospheric pressure (green line); non-slip and impermeability (solid black line), where velocities u and w are null; hydrostatic profile (blue line), which is composed of the outlet pressure BC and characterizing an open flow channel; meanwhile, the average water level is kept constant and equal to h=10.98 m (Fig. 2a) or h_1=10.52 m (Fig. 2b), which prevents the wave channel from emptying and additionally enables the use of a numerical beach (gray region in Fig. 2). The use of such a beach is in accordance with the recommendation of Lisboa et al. (2017) and has a length corresponding to 2λ. Moreover, the prescribed velocity BC (red line in Fig. 2) also is found. While this consists of a continuous segment for the generation of the representative regular waves (Fig. 2), this segment is subdivided into 14 equal segments of size h/14 for generating realistic irregular waves, as recommended by Machado et al. (2021) and Paiva et al. (2023). This approach is illustrated in Figure 3.

A stretched mesh was adopted for spatial discretization (Gomes et al., 2012), in which the computational domain has been subdivided vertically into 3 regions: 1) the region that contains only air and is discretized into 20 computational cells, 2) the free surface region that contains the air/water interface and is discretized into 40 cells, and 3) the region that contains only water and is discretized into 60 cells. Horizontally, the mesh is subdivided into 50 cells per λ, totaling 250 computational cells in the horizontal plane.

As recommended by Machado et al. (2021), the simulations on realistic irregular wave generation uses the time step (Δt) for temporal discretization, which corresponds to Δt=0.05 s. However, the simulations of representative regular wave generation uses a time step of T_m/500 as recommended by Gomes (2014), which corresponds here to Δt=0.0114 s. Finally, all simulations should be noted to consider a total time of 900 s for wave generation and propagation.

When aiming to evaluate the results, probes were used to monitor the free surface elevation in the wave channel and were placed at x=0 m (wave generation zone), 10.45 m; 20.91 m, 31.36 m, 41.82 m, 50.18 m, 60.64 m, 71.09 m (the recommended location for device insertion as per De Lima, 2021), as well as 81.55 m, 92.00 m, and 102.46 m. Subsequently, the results obtained in Ansys Fluent were compared with the series of free surface elevations obtained in TOMAWAC for the cases involving realistic irregular

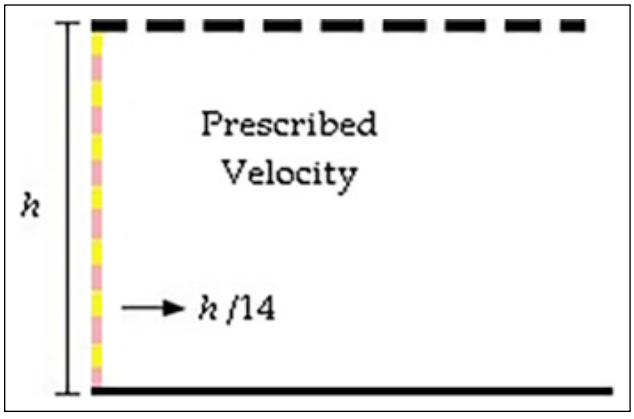

Figure 3. Illustration of the subdivision recommended by Machado et al. (2021).

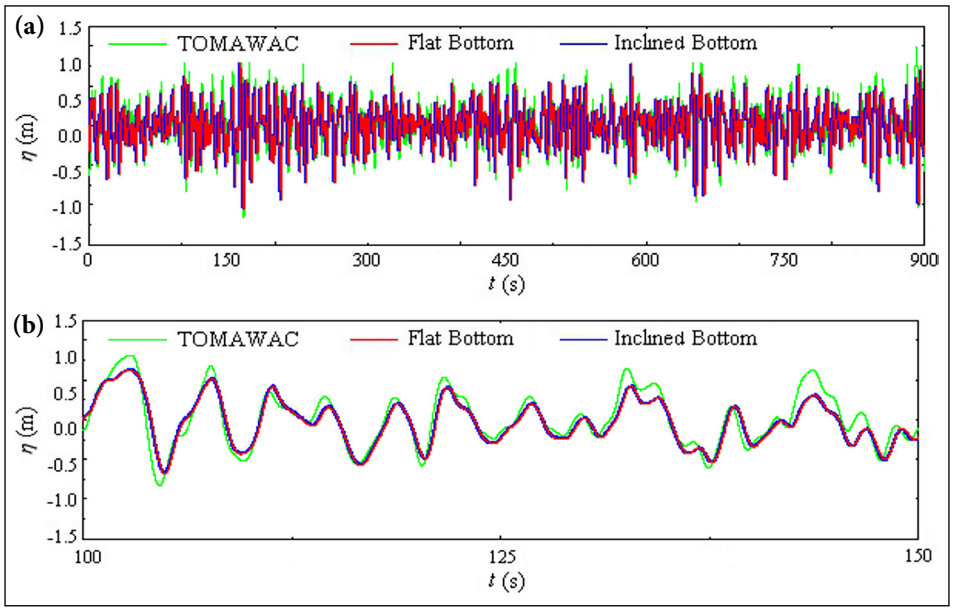

Figure 4. Qualitative comparison of the results obtained in the first analysis considering realistic irregular waves at the probe located at x=0 m: (a) 0 s ≤ t ≤ 900 s; (b) 100 s ≤ t ≤ 150 s.

waves, while the analytical elevation series obtained from Eq. 14 was used for the cases where representative regular waves were generated. In order to quantitatively analyze these results, the metrics MAE (mean absolute error) and RMSE (root mean square error) were taken into consideration and calculated as (Chai & Draxler, 2014):

$$\mathrm{MAE} = \frac{\sum_{i=1}^{N} |O_i - P_i|}{N} \tag{17}$$

$$\mathrm{RMSE} = \sqrt{\frac{\sum_{i=1}^{N} (O_i - P_i)^2}{N}} \tag{18}$$

where N represents the total amount of data, O_i represents the value obtained numerically (m), and P_i is the value used as a reference (m).

4. RESULTS AND DISCUSSIONS

4.1. Analysis of the influence of bathymetry on the generation and propagation of realistic irregular waves

In order to evaluate the differences monitored regarding the generation and propagation of realistic irregular waves in wave channels with flat or inclined bottoms, the free surface elevation was monitored at 11 points along the channels, and two analyses were carried out. The first analysis compared the results with the elevation of the free surface resulting from the TOMAWAC model, thus verifying the generation of realistic irregular waves, while the second analysis compared the numerical results obtained for the two wave channels with each other.

Regarding the first analysis, this verification is highlighted as having been carried out in the generation zone, (i.e., at x=0 m); this was due to a restriction of the WaveMIMO methodology, as TOMAWAC provides data referring only to the location of the study. Thus, MAE was found to be 0.0892 m and RMSE to be 0.1144 m for the wave channel with a flat bottom, while MAE was equal to 0.0889 m and RMSE to 0.1141 m for the wave channel with an inclined bottom.

Figure 4 presents a qualitative comparison of the results from the first analysis considering realistic irregular waves. While Figure 4a has 900 s of simulation, Figure 4b highlights the interval 100 s ≤ t ≤150 s in order to enable better visualization of the results. As can be seen in Figure 4a, the waves that were numerically generated in both channels adequately reproduce the realistic sea state. This can be observed in greater detail in Figure 4b, where only some crests and troughs are noted as having not been reached.

Furthermore, both the quantitative and qualitative results are worth noting to be similar to those found by Machado et al. (2021), Maciel et al. (2021), Cisco et al. (2021), Maciel et al. (2023), and Paiva et al. (2023). Therefore, the generation of the realistic irregular waves found in Tramandaí has been verified through the WaveMIMO methodology. Finally, this analysis corroborates the indication of using a wave channel with an inclined bottom, as the MAE and RMSE metrics obtained are lower than those obtained when considering a wave channel with a flat bottom.

Continuing the discussion of the results, Table 2 presents the MAE and RMSE metrics obtained in the second analysis. The results obtained in this analysis using the wave channel with an inclined bottom are worth noting to have been taken as a reference. This is because the bottom of this channel represents the ocean floor of the studied site.

As seen in Table 2, the lowest values obtained for the MAE and RMSE metrics refer to the central probes, particularly those around the region of the channel that is recommended for inserting the converter (x=71.09 m). When considering this probe and comparing the metrics with H_s, differences of 0.48% for MAE and 0.59% for RMSE are found. Meanwhile,

the highest values found for the probe located at x=102.46 m reveal differences of 0.67% for MAE and 0.87% for RMSE when compared with H_s.

Concluding the second analysis, Figure 5 presents the free surface elevation of the realistic irregular waves monitored at x=71.09 m by considering the wave channels with a flat or inclined bottom. Thus, Figure 5a also shows the full 900 s of the simulation, while Figure 5b highlights the interval 100 s ≤ t ≤200 s.

Qualitatively, the free surface elevation of realistic irregular waves in Figure 5 can be identified as not having been considerably affected by the use of bathymetry in the wave channel, nor are the results in Figure 5b visually distinguishable. Therefore, the present results indicate the use of a wave channel with an inclined bottom, since this more closely represents the characteristics of the seabed at the study site.

Finally, Figure 6 displays the volume fraction field in order to enable the visualization of the physical phenomenon of generating and propagating realistic irregular waves. Thus, Figure 6a presents the wave channel with a flat bottom and Figure 6b the one with an inclined bottom at time t=0 s, whereas Figures 6c and d present the same respectively but at time t=900 s.

Table 2. MAE and RMSE metrics obtained in the second analysis considering the generation and propagation of realistic irregular waves

Probe position (m)	MAE (m)	RMSE (m)
0	0.0057	0.0076
10.45	0.0054	0.0071
20.91	0.0048	0.0063
31.36	0.0045	0.0059
41.82	0.0045	0.0059
50.18	0.0044	0.0057
60.64	0.0042	0.0053
71.09	0.0043	0.0053
81.55	0.0046	0.0059
92.01	0.0054	0.0069
102.46	0.0060	0.0078

MAE: Mean Absolute Error; RMSE: Root Mean Square Error.

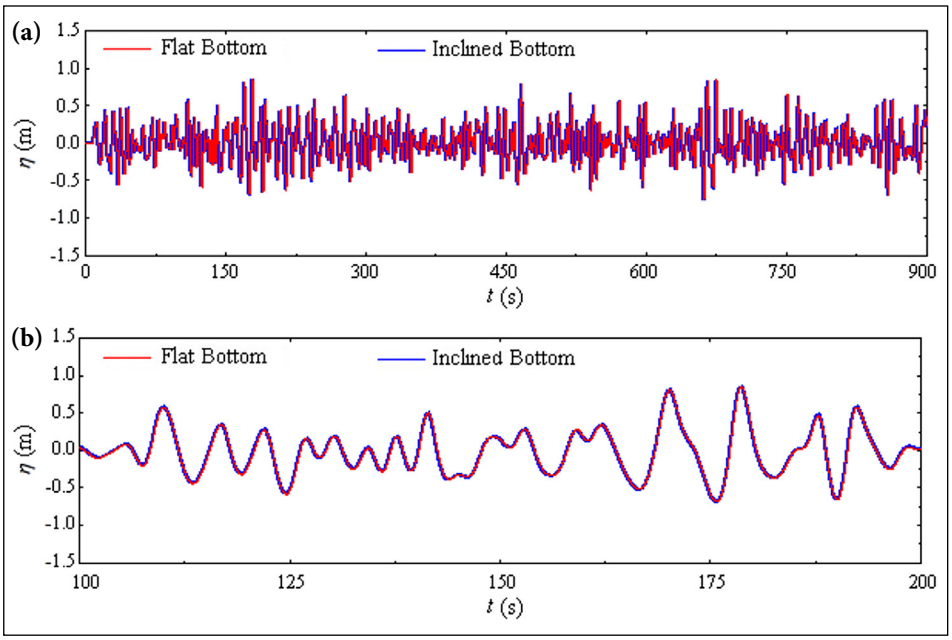

Figure 5. Qualitative comparison of the results obtained in the second analysis considering realistic irregular waves for the probe located at x=71.09 m: (a) 0 s ≤ t ≤ 900 s; (b) 100 s ≤ t ≤ 200 s.

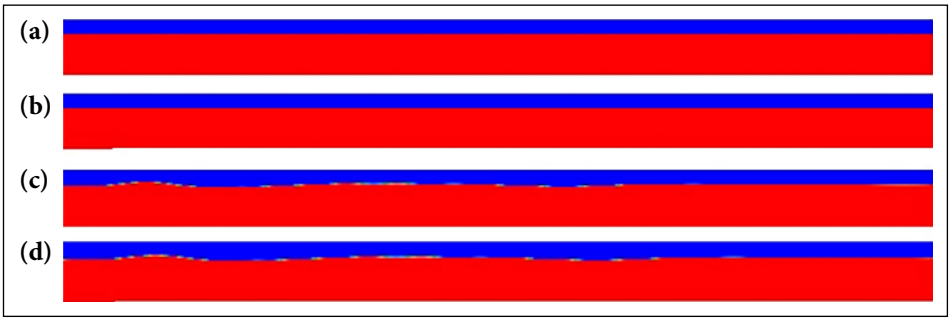

Figure 6. Elevation of the free surface at t=0 s for channels with (a) a flat bottom or (b) an inclined bottom and at t=900 s for channels with (c) a flat bottom or (d) an inclined bottom.

Table 3. MAE and RMSE metrics obtained in the first analysis considering representative regular waves

Probe position (m)	Flat bottom		Inclined bottom	
	MAE (m)	RMSE (m)	MAE (m)	RMSE (m)
0	0.0235	0.0302	0.0235	0.0302
10.45	0.0340	0.0446	0.0340	0.0445
20.91	0.0463	0.0583	0.0461	0.0581
31.36	0.0336	0.0474	0.0332	0.0470
41.82	0.0468	0.0611	0.0458	0.0601
50.18	0.0536	0.0693	0.0521	0.0678
60.64	0.0412	0.0583	0.0396	0.0567
71.09	0.0550	0.0727	0.0521	0.0700
81.55	0.0738	0.0912	0.0698	0.0874
92.01	0.0573	0.0770	0.0527	0.0728
102.46	0.0761	0.0955	0.0699	0.0896

MAE: Mean Absolute Error; RMSE: Root Mean Square Error.

At the initial instant of the simulation (i.e., t=0 s) in Figure 6a and b, due to the state of inertia, the flow was at rest and thus no disturbance occurred at the free surface elevation. However, at t=900 s (Figs. 6c, d), oscillatory movement at the free surface elevations are observable at the end of the simulation. Moreover, the functioning of the numerical beach is also noteworthily observed in Figures 6c and d, with no oscillations occurring at the end of the channel in this damping region.

4.2. Analysis of the influence of bathymetry on the generation and propagation of representative regular waves

To evaluate the differences monitored in the generation and propagation of representative regular waves in wave channels with a flat bottom and an inclined bottom and analogous to the previous experiment in Section 4.1, two analyses have been carried out. The first analysis compares the numerical results that were obtained with the results from the analytical solution using Equation 14, while the second analysis compares the numerical results obtained for channels with an inclined bottom to the results for those with a flat bottom. Therefore, Table 3 presents the MAE and RMSE metrics obtained in the first analysis, which have also been used to verify the generation of representative regular waves.

As observed in Table 3, the free surface elevation that was monitored does not present considerable differences in relation to the analytical results for any of the 11 evaluated probes. Even so, the results are slightly more accurate when the local bathymetry is reproduced in the bottom of the wave channel. As expected, when considering the probe located in the wave generation zone (i.e., at x=0 m), no difference is found between the MAE and RMSE values that were obtained, regardless of bathymetry being used or not, because no inclination occurs at the bottom of channel at this location. Now, for the results monitored at x=41.82 m, the differences between the values obtained for the cases with flat and inclined bottoms are 2.13% for MAE and 1.63% for RMSE.

Moreover, in order to consider the location where the converter devices must be placed in accordance with De Lima (2021), namely at 1.5λ from the wave generation zone, the results obtained at x=71.09 m are evaluated, with differences of 5.56% for MAE and 3.85% for RMSE being found when comparing both simulations. Finally, the difference between the MAE and RMSE metrics found for the cases with flat and those with inclined bottoms is noted to be directly proportional to the position of the monitoring probes.

Continuing the first analysis, Figure 7 shows the free surface elevation obtained at x=41.82 m when considering the representative regular waves generated in wave channels with flat and inclined bottoms, as well as the free surface elevation calculated analytically. Looking at these alongside the results presented in Table 3 enables verification of the numerical wave generation model. Furthermore, this probe position should be highlighted to have been evaluated due to being approximately one wavelength (λ=45.91 m) away from the left wall of the wave channel (i.e., from the wave generation zone).

Qualitatively, Figure 7a reveals the representative regular waves to have been adequately generated, a fact observable in greater detail in Figure 7b, which highlights the period 100 s ≤ t ≤ 200 s. As can be seen in Figure 7a, a difference occurs between the numerical and analytical results at the initial moments. This is due to the flow starting from rest and the first waves generated in the channel being damped due to inertia, leading to deviations when compared with the analytical results. Moreover, the MAE and RMSE metrics presented in Table 3 have been used to confirm the observed results, as well as the appropriate generation of representative regular waves in the wave channels with flat and inclined bottoms.

Concluding the first analysis, Figure 8 presents the free surface elevation of the representative regular waves generated in wave channels with a flat or inclined bottom, as well as the free surface elevation calculated analytically by considering the probe positioned at x=71.09 m.

Qualitatively, Figure 8a reveals the representative regular waves to have been generated appropriately, with this being observable in greater detail in Figure 8b which shows the interval 100 s ≤ t ≤200 s. Furthermore, for t ≤20 s in Figure 8a, a difference is found between the numerical and analytical results. This is due to inertia, just as noted in the previous case. Quantitatively, the MAE and RMSE metrics presented in Table 3 are used to confirm the observed results and again have been able to verify the appropriate generation and propagation of representative regular waves in wave channels with flat and inclined bottoms.

Table 4 presents the MAE and RMSE metrics obtained regarding the second analysis, which compares the free surface elevation data monitored along the flat-bottom and inclined-bottom wave channels with each other. As mentioned, the results found for the case where bathymetry is reproduced at the bottom of the wave channel was adopted as a reference for this analysis.

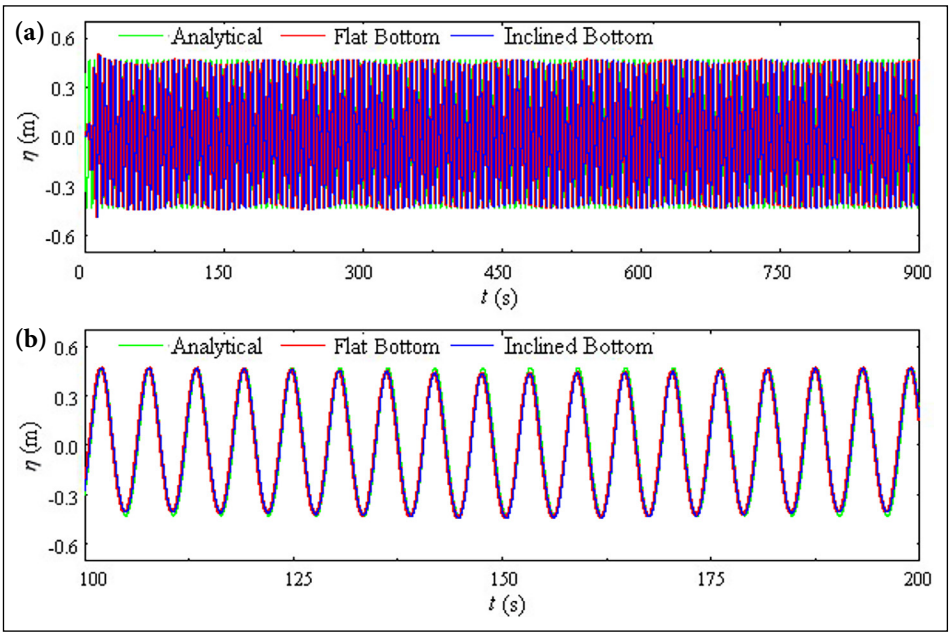

Figure 7. Qualitative comparison of the results obtained in the first analysis considering representative regular waves at the probe located at x=41.82 m: (a) 0 s ≤ t ≤ 900 s; (b) 100 s ≤ t ≤ 200 s.

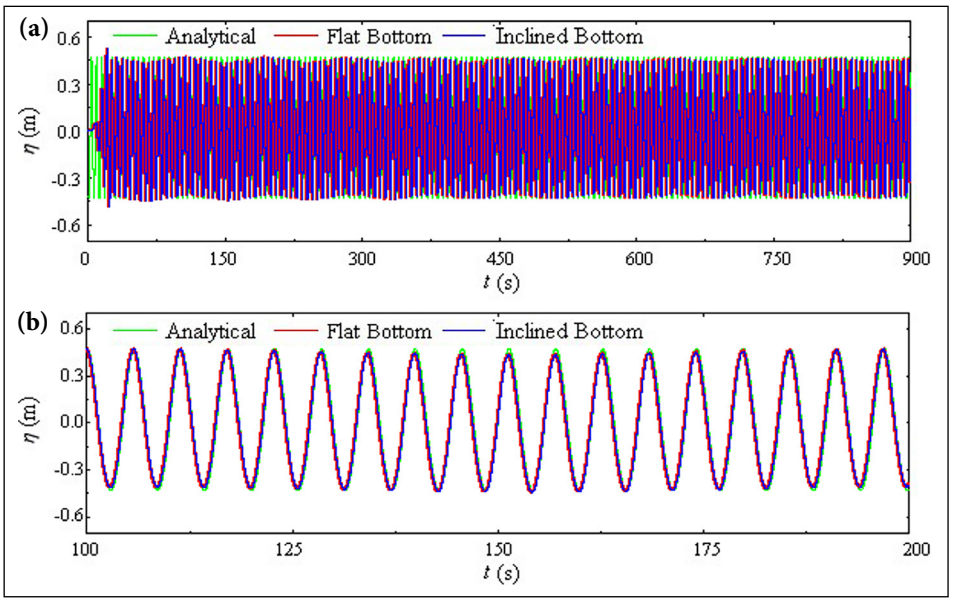

Figure 8. Qualitative comparison of the results obtained from the first analysis considering representative regular waves at the probe located at x=71.09 m: (a) 0 s ≤ t ≤ 900 s; (b) 100 s ≤ t ≤ 200 s.

As seen in Table 4, the smallest differences are found in the first 7 probes positioned on the wave channel; this is due to the bathymetry having little interference in this region, with the bottom inclination varying between 0.094 m and 0.098 m there. As in the first analysis, the MAE and RMSE metrics are noted to be directly proportional to the inclination of the channel bottom. Furthermore, when comparing the MAE and RMSE metrics with H_s, differences of 0.12% for MAE and 0.15% for RMSE are found at x=0 m, of 0.48% for MAE and 0.59% for RMSE at x=71.09 m, and of 0.77% for MAE and 0.90% for RMSE at x=102.46 m. Lastly, the results from the two analyses suggest including bathymetry when considering representative regular waves in a wave channel.

To conclude the presentation results, Figure 9 displays the fluid dynamic behavior of generating and propagating representative regular waves. Thus, Figure 9a shows the volume fraction field for the wave channel with a flat bottom and Figure 9b for the one with an inclined bottom at time t=0 s, while Figures 9c and d show the same respectively but at time t=900 s. As in the previous case (Fig. 6), the fluids are notably at rest at the initial instant in the simulation (i.e., at t=0 s; Figs. 9a, b). However, the oscillatory movement shown at the end of the simulation (i.e., at t=900 s; Figs. 9c, d) presents regular behavior. Moreover, the functioning of the numerical beach can be observed again at the end of the channel.

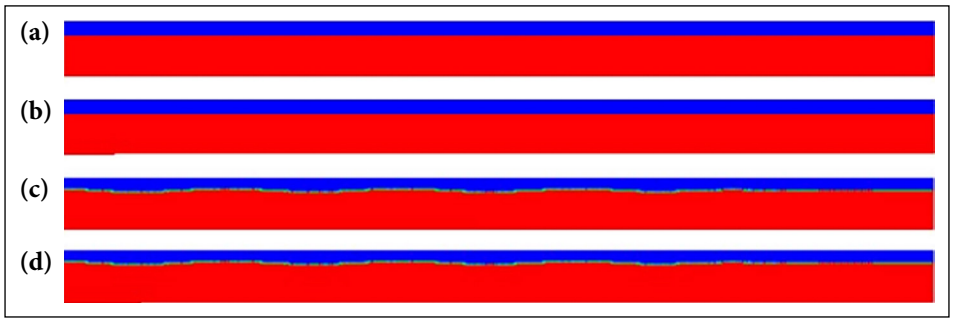

Figure 9. Elevation of the free surface at t=0 s for channels with: (a) a flat bottom; (b) an inclined bottom, also at t=900 s for channels with: (c) a flat bottom; (d) an inclined bottom.

5. CONCLUSION

As mentioned, the objective of the present study has been to evaluate the influence of the bathymetry of a wave channel on the generation and propagation of realistic irregular waves and on the representative regular waves for the sea conditions found in the municipality of Tramandaí, RS, Brazil. Therefore, numerical simulations have been carried out by considering wave channels with a flat bottom where the bathymetry was not taken into account, as well as wave channels with an inclined bottom where the local bathymetry has been reproduced.

The first investigation used wave channels to generate and propagate realistic irregular waves and was carried out using the WaveMIMO methodology (Machado et al., 2021). For both the simulations that were carried out, the realistic sea state coming from the TOMAWAC spectral model was seen to have been adequately reproduced. Thus, the channel bottom was observed to present little influence over the generation of realistic irregular waves. However, reproducing the bathymetry resulted in slightly better results. Regarding the free surface elevation monitored in the wave generation zone at x=0 m, the difference between the evaluated metrics for the case with a flat bottom and the case with an inclined bottom was 0.33% for MAE and 0.26% for RMSE.

The second investigation used wave channels to simulate the generation and propagation of representative regular waves of the sea conditions that occurred in Tramandaí. When compared with the analytical solution, the numerical model that had been employed was able to reproduce the wave climate in both investigated channel types. The waves generated in the channel with an inclined bottom were also observed to show improved accuracy; when considering the probe at x=41.82 m, the difference between the metrics for the cases with a flat bottom and an inclined bottom were 2.13% for MAE and 1.63% for RMSE. Meanwhile, for the probe at x=71.09 m, differences of 5.56% for MAE and 3.85% for RMSE were found.

In conclusion, this study has been able to identify a theoretical recommendation for using wave channels with an inclined bottom, namely those that reproduce the bathymetry of a study site. Furthermore, future studies are suggested to be carried out that evaluate the influence of bathymetry at the bottom of the wave channel with regard to the performance of wave energy converter devices.

Table 4. MAE and RMSE metrics obtained in the second analysis considering representative regular waves

Probe position (m)	MAE (m)	RMSE (m)
0	0.0010	0.0013
10.45	0.0034	0.0042
20.91	0.0034	0.0042
31.36	0.0034	0.0042
41.82	0.0035	0.0043
50.18	0.0036	0.0044
60.64	0.0038	0.0047
71.09	0.0043	0.0053
81.55	0.0048	0.0059
92.01	0.0059	0.0070
102.46	0.0069	0.0081

MAE: Mean Absolute Error; RMSE: Root Mean Square Error.

DATA AVAILABILITY STATEMENT

The published publication includes all graphics and data collected or developed during the study.

CONFLICT OF INTEREST

The author declared no potential conflicts of interest with respect to the research, authorship, and/or publication of this article.

ETHICS

There are no ethical issues with the publication of this manuscript.

USE OF AI FOR WRITING ASSISTANCE

Used only to check the writing of the text in English.

FINANCIAL DISCLOSURE

A. P. G. M. and M. S. P. thank CNPq and CAPES (Funding Code 001) for their scholarships. L. A. O. R., E. D. d. S., and L. A. I. thank CNPq for their research grants (Processes: 307791/2019-0; 308396/2021-9; and 309648/2021-1, respectively). B. N. M. is grateful for the financial support from the institutional research assistance program for newly hired professors at the Federal University of Rio Grande do Sul. All authors thank FAPERGS (Public Call FAPERGS 07/2021 - Programa Pesquisador Gaúcho (PqG), Process: 21/2551-0002231-0) and CNPq (Public Call CNPq/MCTI Nº 10/2023 – Universal, Process: 403408/2023-7).

REFERENCES

Cannata, G., Simone, M., & Gallerano, F. (2023) Numerical investigation into the performance of an OWC device under regular and irregular waves. *Journal of Marine Science and Engineering, 11*(4), Article 735. [CrossRef]

Cardoso, S. D., Marques, W. C., Kirinus, E. D. P., & Stringari, C. E. (2014). *Levantamento batimétrico usando cartas náuticas*. In 13ª Mostra da Produção Universitária, Universidade Federal do Rio Grande. [Portuguese]

Chakrabarti, S. K. (2005). *Handbook of offshore engineering*. Elsevier.

Chai, T., & Draxler, R. R. (2014). Root mean square error (RMSE) or mean absolute error (MAE)? - Arguments against avoiding RMSE in the literature. *Geoscientific Model Development, 7*(3), 1247–1250. [CrossRef]

Cisco, L. A., Koch, A. H. S., Condotta, M. P., Hofstatter, R., Harras, L. M., Oleinik, P. H., Paiva, M. S., Isoldi, L. A., & Machado, B. N (2020). O oceano como fonte de energia: uma revisão da literatura. *Revista Interdisciplinar de Pesquisa em Engenharia, 6*(2), 23–33. [Portuguese]

Dean, R. G., & Dalrymple, R. A. (1991). *Water wave mechanics for engineers and scientists*. World Scientific Publishing Company. [CrossRef]

De Lima, Y. T. B. (2021). Análise geométrica através do design construtal de conversores de energia das ondas do mar do tipo coluna de água oscilante com câmaras hidropneumáticas acopladas. Tese de doutorado em engenharia mecânica, Universidade Federal do Rio Grande do Sul. [Portuguese]

EPE (2023). Brazilian Energy Balance 2023. Ministry of Mines and Energy, Rio de Janeiro. Available online: https://www.epe.gov.br/pt/publicacoes-dados-abertos/publicacoes/balanco-energetico-nacional-2023. Accessed on Oct 04, 2023).

Gomes, M. D. N., Isoldi, L. A., Santos, E. D. D., & Rocha, L. A. O. (2012). *Análise de malhas para geração numérica de ondas em tanques*. In Anais do VII do Congresso Nacional de Engenharia Mecânica (Associação Brasileira de Engenharia e Ciências Mecânicas). [Portuguese].

Gomes, M. N. (2014). *Constructal Design de dispositivos conversores de energia das ondas do mar em energia elétrica do tipo Coluna de Água Oscilante*. Tese de doutorado em engenharia mecânica, Universidade Federal do Rio Grande do Sul. [Portuguese].

Hirt, C. W., & Nichols, B. D. (1981). Volume of fluid (VOF) method for the dynamics of free boundaries. *Journal of Computational Physics, 39*(1), 201–225. [CrossRef]

Hübner, R. G., Fragassa, C., Paiva, M. D. S., Oleinik, P. H., Gomes, M. D. N., Rocha, L. A., dos Santos, E. D., Machado, B. N., & Isoldi, L. A (2022). Numerical analysis of an overtopping wave energy converter subjected to the incidence of irregular and regular waves from realistic sea states. *Journal of Marine Science and Engineering, 10*(8), Article 1084. [CrossRef]

IEA (2024). *Renewables 2023, IEA, Paris* https://www.iea.org/reports/renewables-2023, Licence: CC BY 4.0.

Koch, A. H. S., Paiva, M. S., Monteiro, C. B., Oleinik, P. H., Isoldi, L. A., & Machado, B. N. (2021). Numerical evaluation of the hydropneumatic power of the oscillating water column wave energy converter submitted to regular and irregular waves. *Engineering Science & Technology, 3*, 32–43. [CrossRef]

Lisboa, R. C., Teixeira, P. R. F., & Didier, E. (2017). Regular and irregular wave propagation analysis in a flume with numerical beach using a navier-stokes based model. *Defect and Diffusion Forum, 372*, 81–90. [CrossRef]

Maliska, C. R. (2004). *Tranferência de Calor e Mecânica dos Fluidos Computacional*. LTC - Livros Técnicos e Científicos. [Portuguese]

Maciel, R. P., Fragassa C., Machado, B. N., Rocha, L. A. O., Dos Santos, E. D., Gomes, M. N., & Isoldi, L. A. (2021). Verification and validation of a methodology to numerically generate waves using transient discrete data as prescribed velocity boundary condition. *Journal of Marine Science and Engineering, 9*(8), Article 896.

Maciel, R. P., Oleinik, P. H., Dos Santos, E. D., Rocha, L. A. O., Machado, B. N., Gomes, M. N., & Isoldi, L. A (2023). Constructal design applied to an oscillating water column wave energy converter device under realistic sea state conditions. *Journal of Marine Science and Engineering, 11*(11), Article 2174. [CrossRef]

Machado, B. N., Oleinik, P. H., Kirinus, E. P., Dos Santos, E. D., Rocha, L. A. O., Gomes, M. N., Conde, J. M. P., & Isoldi, L. A. (2021). WaveMIMO Methodology: Numerical wave generation of a realistic sea state. *Journal of Applied and Computational Mechanics, 7*(4), 2129–2148.

Oleinik, P. H. (2022). O programa Spec2Wave: Manual do usuário. *RIPE 6*(2), 23–33. [Portuguese]

Oleinik, P. H., Tavares, G. P., Machado, B. N., & Isoldi, L. A. (2021). Transformation of water wave spectra into time series of surface elevation. *Earth, 2*(4), 997–1005. [CrossRef]

Paiva, M. S., Mocellin, A. P. G., Koch, A. H. S., Oleinik, P. H., Isoldi, L. A., & Machado, B. N. (2023). Investigation on the Discretization of the Realistic Irregular Wave Generation Region through the WaveMIMO Methodology. *Revista de Engenharia Térmica, 22*(1), 3–10. [CrossRef]

Palma, G., Formentin, S. M., Zanuttigh, B., Contestabile, P., & Vicinanza, D. (2019). Numerical simulations of the hydraulic performa3nce of a breakwater-integrated overtopping wave energy converter. *Journal of Marine Science and Engineering, 7*(2), Article 38. [CrossRef]

Pecher, A. & Kofoed, J. P (2017). Handbook of ocean wave energy. Springer Nature. [CrossRef]

Seibt, F. M., Dos Santos, E. D., Isoldi, L. A., & Rocha, L. A. O. (2023). Constructal Design on full-scale numerical model of a submerged horizontal plate-type wave energy converter. Marine Systems and Ocean Technology Key, *18*, 1–13. [CrossRef]

Santana, D. R. (2023). Energia Renovável para o Desenvolvimento Econômico do Brasil. *Revista OWL - Revista Interdisciplinar de Ensino e Educação, 1*(1), 48–64. [Portuguese]

Versteeg, H. K., & Malalasekera, W. (2007). *An introduction to computational fluid dynamics - The finite volume method*. Pearson Education Limited.